

## Property profile development during wire extrusion and wire drawing of magnesium alloys AZ31 and ZX10

Nienaber, Maria; Braatz, Merle; Ben Khalifa, Noomane; Bohlen, Jan

*Published in:*  
Materials and Design

*DOI:*  
[10.1016/j.matdes.2022.111355](https://doi.org/10.1016/j.matdes.2022.111355)

*Publication date:*  
2022

*Document Version*  
Publisher's PDF, also known as Version of record

[Link to publication](#)

*Citation for pulished version (APA):*  
Nienaber, M., Braatz, M., Ben Khalifa, N., & Bohlen, J. (2022). Property profile development during wire extrusion and wire drawing of magnesium alloys AZ31 and ZX10. *Materials and Design*, 224, Article 111355. <https://doi.org/10.1016/j.matdes.2022.111355>

### General rights

Copyright and moral rights for the publications made accessible in the public portal are retained by the authors and/or other copyright owners and it is a condition of accessing publications that users recognise and abide by the legal requirements associated with these rights.

- Users may download and print one copy of any publication from the public portal for the purpose of private study or research.
- You may not further distribute the material or use it for any profit-making activity or commercial gain
- You may freely distribute the URL identifying the publication in the public portal ?

### Take down policy

If you believe that this document breaches copyright please contact us providing details, and we will remove access to the work immediately and investigate your claim.



# Property profile development during wire extrusion and wire drawing of magnesium alloys AZ31 and ZX10

Maria Nienaber<sup>a,\*</sup>, Merle Braatz<sup>a</sup>, Noomane Ben Khalifa<sup>a,b</sup>, Jan Bohlen<sup>a</sup>

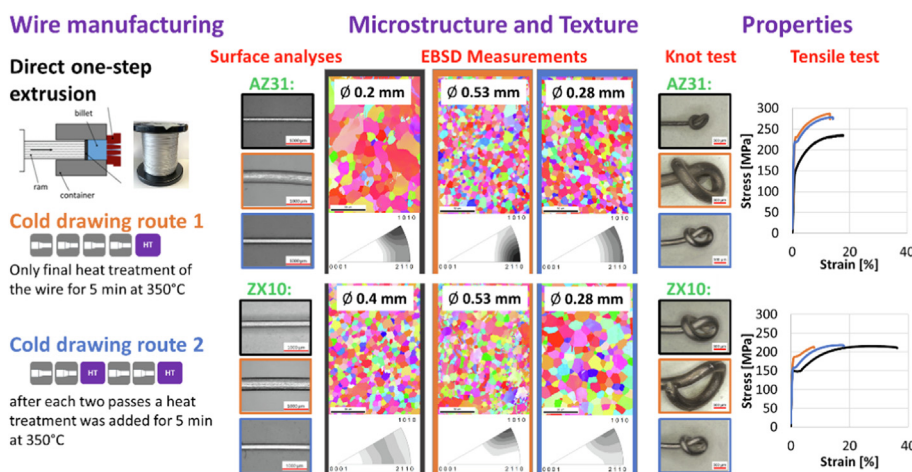
<sup>a</sup> Institute of Material and Process Design, Helmholtz-Zentrum Hereon, Max-Planck-Str. 1, 21502 Geesthacht, Germany

<sup>b</sup> Institute of Product and Process Innovation, Leuphana Universität Lüneburg, Universitätsallee 1, 21335 Lüneburg, Germany

## HIGHLIGHTS

- Direct comparison of property profiles depending on the manufacturing process and alloy.
- One-step direct extrusion of wires up to a diameter of 0.2 mm.
- DRX is the dominant mechanism for texture development in extrusion and SRX in wire drawing, resulting in different property profiles.
- Improvement of the properties significantly by drawing, especially after the first two passes.

## GRAPHICAL ABSTRACT



## ARTICLE INFO

### Article history:

Received 4 October 2022

Revised 6 November 2022

Accepted 7 November 2022

Available online 8 November 2022

### Keywords:

Magnesium wire

Extrusion

Drawing

AZ31

ZX10

Property design

## ABSTRACT

This paper deals with the impact of the wire manufacturing process on the mechanical property development of two magnesium alloys, AZ31 and ZX10. For this study, wires were produced with different diameters of up to 0.2 mm via direct one-step extrusion as a hot forming route and were directly compared to conventional cold drawing manufacturing routes with diameters up to 0.3 mm and associated heat-treatment. The alloy dependent microstructure development is resolved with respect to the underlying recrystallization mechanisms, which determines the texture development and concurrently the strength and ductility properties of the wires. The experimental results clearly show that the manufacturing process, the degree of deformation (wire diameter) as well as the alloy itself have a major impact on the texture development and mechanical properties of the wires. While AZ31, does not enable a strong impact on the microstructure development, ductility in ZX10 is enhanced with a concurrent weak texture development due to adjusted dynamic recrystallization during hot forming. In contrast, such microstructures cannot be adjusted in the cold forming routes due to static recrystallization. However, it is possible to improve the properties significantly by drawing, which is limited by the first two drawing passes. © 2022 The Authors. Published by Elsevier Ltd. This is an open access article under the CC BY license (<http://creativecommons.org/licenses/by/4.0/>).

\* Corresponding author.

E-mail address: [Maria.Nienaber@hereon.de](mailto:Maria.Nienaber@hereon.de) (M. Nienaber).

## 1. Introduction

Metallic wires of magnesium alloys are nowadays associated with biomaterial applications in the form of sutures or specific stent solutions due to the distinct degradation behaviour of this class of materials [1–3]. Earlier positions in this field address the benefit of using magnesium alloy wires as biodegradable materials leading back into 19th century applications [4] while also addressing the lack of adjusted ductility for such applications [5,6]. Actual applications, e.g. connections with surgical wires, foresee the ability to manual pulling of the wires during bones fixture as well as wire fastening e.g. based on twisting or knotting the wires [7,8]. A consistent homogeneous mechanical property profile and high ductility is therefore essential where deformation is applied, especially during insertion but also during service [9]. Unfortunately, magnesium and its alloys are often discussed as less formable compared to other conventional alloys; an established view often associated with the hexagonal lattice structure of the material [10,11]. In addition, the massive forming of magnesium leads to the development of a distinct crystallographic texture with a strong orientation of the basal, which is not supportive of good formability [12,13]. There are various methods to change the texture and so the material properties. The main influence on the texture, beside the alloy composition, is the manufacturing process, which is related to the dominant recrystallization mechanisms (static recrystallization (SRX) or dynamic recrystallization (DRX)) [14–18]. For flat products, it is well known that the manufacturing process, such as rolling or extrusion, determines an alloy dependent microstructure and texture development with direct impact on the mechanical property profile [14,19].

In terms of magnesium wire production, there are also various methods of manufacturing them. A common method for producing thin wires is the application of drawing processes to thin extruded rods [20–25]. However, direct extrusion also offers the possibility of producing wires [26–29]. In the current literature, the research focus is on the influence of the alloy on the properties for medical applications [1,2,20,30–33] and on possible manufacturing processes of wires [26,34–36]. But there is no direct alloy-dependent comparison of the influence of the manufacturing process on wire's property profiles.

Therefore, the aim of this work is to contribute to the understanding of the influence of the wire manufacturing process on their properties. In addition, the previous studies on direct extrusion of wire show only very limited possibility of economic professional production of wire, because they extrude with only a very low extrusion ratio, unlike in this study.

The manufacturing of wires by wire drawing itself is typically based on a complex multistep wire drawing process, which includes cold drawing passes and intermediate heat treatment. Starting e.g. with a pre-extruded round bar or wire, concurrent drawing passes are used for wire thinning including intermediate softening due to static recovery and SRX. The drawing process is comparable to a rolling process. Thus, the microstructure development may also be different compared to a hot forming route such as extrusion. During cold forming, where DRX is restricted (e.g. as it has been observed during sheet rolling of magnesium alloys [18] or multi-pass cold drawing [37]), the resulting microstructures and textures as well as their development during a static recrystallization (SRX) driven heat treatment can differ distinctly. During wire drawing, static recrystallization dominates.

Wire extrusion is a single-step forming process in which the degree of deformation is much higher than in rolling and DRX is dominating. Studies have shown that the degree of forming has an influence on the recrystallization behaviour, which usually leads to a smaller grain size and a decreasing texture intensity

[26,38]. During hot forming, such as extrusion, the kinetics of recrystallization will be determined by the processing parameter settings, especially the temperature, speed and the extrusion ratio, which determine how far the recrystallization mechanism is developing along with the microstructure development [15–17,39].

In addition to the manufacturing process, the alloying also influences the texture and thus the properties of the material. Such texture weakening has been described for alloys with rare earth (RE) elements or calcium as alloying elements where enhanced non-basal slip during massive forming [40–42] as well as a change of the dominating mechanisms recrystallization [12,13,43] lead to weaker textures and therefore higher ductility of the formed parts. Therefore, it is important to understand both the influence of the alloy but also the influence of the manufacturing process.

To achieve the aim of this study, wires were manufactured along two processing routes. One being hot forming by direct extrusion (DRX is dominating), the other one being cold wire drawing in multiple passes including a variation of a heat treatment (SRX is dominating). This allows to investigate direct the alloy dependent influence of the RX-mechanism on the microstructure and texture development and so on the mechanical properties. To show the impact of the alloy, conventional AZ31 and a Ca-containing alloy ZX10 have been chosen. AZ31 is a widely researched well-known reference alloy. ZX10, on the other hand, shows the typical RE effect and is also often used for medical applications.

## 2. Materials and methods

The two magnesium alloys considered in this study were available in the form of cast ingots. While AZ31 was used in the form of a base material, the ZX10 alloy was composed from pure Mg, Zn, and Ca elements and cast into cylinders by applying a modified gravity casting process with lowering the melt into a water bath for directional solidification. The chemical compositions, measured by using X-ray micro fluorescence (M4 Tornado, Bruker), are collected in Table 1.

Billets were machined to a length of 150 mm and a diameter of 49 mm for extrusion of wires with 1 mm diameter. For the extrusion of thinner wires, the billet length was reduced to 75 mm. A solid solution heat treatment was carried out for 16 h at 400 °C followed by air cooling. Direct extrusion of wires was achieved by conventional extrusion, using an automatic 2.5 MN extrusion press (Müller Engineering GmbH & Co. KG, Todtenweis/Sand, Germany). The billets were preheated for 60 min to the extrusion temperature of 400 °C. Dies used for the extrusion experiments consist of 4 nozzles with the same diameter, but varying from 1 mm diameter down to 0.2 mm diameter. Thus, four wires were extruded at the same time during extrusion and an automatic coiler has been used to coil the wires. The initial ram speed of 0.2 mm/s for the 1 mm wire during the direct extrusion experiments has been reduced with decreasing wire diameter in order to remain within the technical limits for the coiling speed. In any case, the realized flow speed is not fully controllable at these high degrees of deformation and is recalculated after the extrusion experiments. Details of the setup and the experimental scheme have been presented in an earlier work [26].

**Table 1**  
Chemical composition of the alloys in this study; values in wt. %; Mg balance.

| Alloy | Al   | Zn   | Ca   | Mn   |
|-------|------|------|------|------|
| AZ31  | 2.88 | 0.90 | –    | 0.21 |
| ZX10  | –    | 0.94 | 0.15 | –    |

An experimental setup for flexible wire drawing processes has been used to carry out multiple cold wire drawing passes using the pre-extruded 1 mm wires. For the conventional wire drawing, the drawing speed is set to 10 mm/s and a die is chosen from the die set that is closest to the targeted diameter reduction ratio  $R$  of 20 % per pass. Before every drawing pass, the wire was pointed manually for threading through the die and then the wire was mounted to the drawing spool of the setup [34]. No lubrication was used. Two different routes were carried out to produce the wires: route 1 without any intermediate heat treatment between passes, but one heat treatment after the final drawing pass, and route 2 with intermediate heat treatments after every second drawing pass. route 1 was done for as many passes as the wires could be drawn. route 2 was terminated after the wire diameter reached 0.3 mm. This is a common target diameter for medical applications [44] and also corresponds to the typical wall thicknesses of ureteral stent [45].

Microstructure and texture analysis of the wires were carried out using electron backscatter diffraction (EBSD) measurements with a field emission scanning electron microscope (SEM) Zeiss Crossbeam 550L equipped with an EDAX-TSL OIM™ system. An acceleration voltage of 15 kV was used and the measurements were carried out with a step size of 0.35  $\mu\text{m}$ . The measuring area and magnification were adapted to the wire diameter. The measuring length in x-direction is at least 1/2 of the wire diameter. The measuring length in the y-direction is 3 times the measuring length in the x-direction. The average grain size and the texture were determined from the entire measuring area. A representative section of 80 by 120  $\mu\text{m}$  was chosen to represent the microstructure. High angle grain boundaries (HAGB, with misorientation angles larger than  $12^\circ$ ) are marked in black. Sample preparation was based on conventional metallographic procedures such as grinding and polishing, giving respect to the small cross-sectional dimensions of the samples. Additional electro-polishing was carried out using Struers AC2™ solution cooled to  $-20^\circ\text{C}$  for 25 s at a voltage of 10 V. For removing the oxide layer on the sample surfaces nitric acid was used.

The mechanical properties of the wires were revealed from tensile tests using the 5 kN universal testing machine of Zwick™ at ambient temperature. A gauge length of 50 mm and a strain rate of  $10^{-3} \text{ s}^{-1}$  were kept constant for the experiments. The strain was detected via the displacement. A simple „knot test“ is adopted in order to analyse the ability of the wire to withstand non-uniaxial straining [8]. For this, a knot is formed manually with a diameter of 7 mm. The ends of the wire are clamped into the above mentioned testing machine and stress is applied using a strain rate of  $10^{-2} \text{ s}^{-1}$  until the fracture of the sample, which occurs in the vicinity of the knot. The ratio of the fracture stress to the ultimate tensile stress (UTS) is a stress ratio used to analyse the ability of the material to maintain its ductility in this more complex forming configuration.

A confocal laser-scanning microscope VK-1000 (Keyence) was used for an optical surface characterization and the determination of the roughness in accordance with DIN EN ISO 25178–2. The mean arithmetic height ( $S_a$ ) was taken from the evaluation as an area related value of the deviation of the surface height compared to its arithmetic mean value. Filter settings were also in accordance with the norm DIN EN ISO 25178–3 with the low pass filter (S filter) set to 0.8  $\mu\text{m}$  and the high-pass filter (L-filter) set to 0.05 mm. Three area measurements of 100  $\mu\text{m}$  x 100  $\mu\text{m}$  each were carried out.

### 3. Results

Hot extrusion experiments at  $400^\circ\text{C}$  for wire diameters of 1 mm, 0.6 mm and 0.4 mm for alloy AZ31 have been carried out successfully. When extruding the wires with a diameter of 0.2 mm, the force limit of the extrusion press has been exceeded and no stable material flow was achieved, although some wires were available for ongoing analysis. The same upper force limit permitted extrusion of 0.4 mm wire diameter for the ZX10 alloy, but several cold cracks occurred during processing, limiting the possibility of wire production. A collection of the wire extrusion parameters and average grain sizes of the wires are shown in Table 2. In order to correlate process parameters to the developing microstructure, the realized exit speed appears to be an appropriate value, as it relates directly to the strain rates achieved in the forming zone during extrusion. For AZ31 wire extrusions, the realized exit speeds are very similar, only slightly lower for the 0.6 mm diameter wire, but significantly lower for the 0.2 mm diameter wire as a result of the reached force limit of the extrusion press. However, the resulting grain size is distinctly lower for the 0.4 mm wire, but increases again when the wire is thinner at 0.2 mm. It is noteworthy that two effects on the microstructure development need to be considered at this point, one being the impact of DRX during the forming process, another one a limited continuation of microstructure development, i.e. grain growth, due to subsequent cooling of the hot extruded wires at air contact. The 0.4 mm wire, with an exit velocity comparable to the thicker wires and despite the significantly higher degree of deformation, has a smaller grain size compared to the 0.6 and 1.0 mm wire. The hypothesis for this effect is that due to the smaller wire diameter, the cooling of the wire is faster and thus the grain growth is strongly limited, resulting in a smaller grain size. The 0.2 mm wire does not continue this effect with a significantly larger grain size. Hypothetically, this would be explained with a lower exit speed allowing a further dynamic grain growth while earlier works have related such effects more to a deformation related forming heat if the temperature or exit speed increases [46–48]. This obviously does not apply in the present case for the extruded AZ31 wires. In case of ZX10 the thinner wires with 0.6 mm and 0.4 mm diam-

**Table 2**  
Experimental data from wire extrusion and resulting average grain sizes corresponding to Fig. 1.

| Alloy | Wire diameter [mm] | Temperature [ $^\circ\text{C}$ ] | Set ram speed [mm/s] | Realized exit speed [m/min] | Average grain size [ $\mu\text{m}$ ] |
|-------|--------------------|----------------------------------|----------------------|-----------------------------|--------------------------------------|
| AZ31  | 1                  | 400                              | 0.2                  | 9.5                         | 8.5                                  |
| AZ31  | 0.6                | 400                              | 0.1                  | 8.7                         | 9.8                                  |
| AZ31  | 0.4                | 400                              | 0.06                 | 9.8                         | 6.3                                  |
| AZ31  | 0.2                | 400                              | 0.03                 | 2.6*                        | 10.8                                 |
| ZX10  | 1                  | 400                              | 0.2                  | 6.0                         | 14.5                                 |
| ZX10  | 0.6                | 400                              | 0.1                  | 3.7                         | 10.8                                 |
| ZX10  | 0.4                | 400                              | 0.06                 | 3.6                         | 5.2                                  |

\*recalculated from ram speed.



eter are comparable regarding the exit speed whereas the 1 mm wire was faster extruded at almost twice the exit speed. Concurrently, the average grain size decreases with the wire thickness.

Fig. 1 shows orientation maps from EBSD measurements to reveal the grain structure of the extruded wires and the corresponding textures in the form of inverse pole figures parallel to the wire extrusion direction. As revealed in previous work [26], strong similarities to extruded round bars are evident. In all cases fully recrystallized microstructures with a uniform equi-axed grain structure are found where only the average grain sizes vary as presented above. Only in case of the 0.2 mm thin AZ31 wire, a rather bimodal microstructure is observed with a number of larger grains embedded into a finer-grained grain structure. While in this condition, a  $\langle 10\text{--}10 \rangle$  fibre component dominates the texture, the thicker AZ31 wires reveal typical recrystallization textures [49] with double-fibre along the arc between the  $\langle 10\text{--}10 \rangle$ - and the  $\langle 11\text{--}20 \rangle$ -poles. After GOS separation of the microstructure of the 0.2 mm wire, it can be seen that it is only partly recrystallized, which also explains the larger grain size compared to the 0.4 mm wire. The texture for GOS greater than 1 shows the well-known deformation texture ( $\langle 10\text{--}10 \rangle$ - component) in the non-recrystallized microstructure.

In contrast, the ZX10 wires show a clear change in textures with decreasing wire diameter. While the 1 mm wire also exhibits a weak preference for a  $\langle 11\text{--}20 \rangle$  fibre component, thinner wires show textures with tilt of basal planes out of the extrusion direction and orientations associated with a “RE texture component”. This texture development has been shown in round bar extrusions of the same alloy [15], but at higher extrusion temperatures a typ-

ical recrystallization texture with  $\langle 11\text{--}20 \rangle$  fibre component has also been observed [50]. In the present case the texture change appears to occur concurrent to a restricted ability of grain growth during the hot forming process.

Cold-drawing experiments of the two alloys were carried out using the extruded wires with 1 mm thickness as starting material. The reduction in the cross-sectional area has been kept constant at  $\sim 20\%$  per drawing pass and for route 2, the wires were taken and heat treated for 5 min at  $350^\circ\text{C}$  after each two passes ( $400^\circ\text{C}$  were not chosen in order to maintain fine-grained microstructures and to keep the heat treatment duration controllable, i.e. not too short). For route 1, the same heat treatment was done once after the final drawing pass.

In summary, it was possible to carry out six passes in sequence for route 1 for both alloys before the material failed in a follow-up pass. Orientation maps from EBSD measurements of route 1 for three feasible drawing schedules are collected in Fig. 2. Again, fully recrystallized microstructures are observed with a uniform equi-axed grain structure. The grain size variations are small, which may be expected due to the same applied heat treatment despite the different strain hardened condition after cold drawing. For both alloys very similar fine grain sizes averaging between 5 and  $6\text{ }\mu\text{m}$  are revealed, which is finer-grained compared to the extruded wires and also does not transport the difference in the developing grain size of the two alloys mentioned before. For AZ31, a preferential strengthening of the  $\langle 11\text{--}20 \rangle$  fibre component is found with increasing number of drawing passes at the expense of an initial  $\langle 10\text{--}10 \rangle$  fibre component. However, for ZX10 such a change is not observed, but the  $\langle 10\text{--}10 \rangle$  fibre component is main-

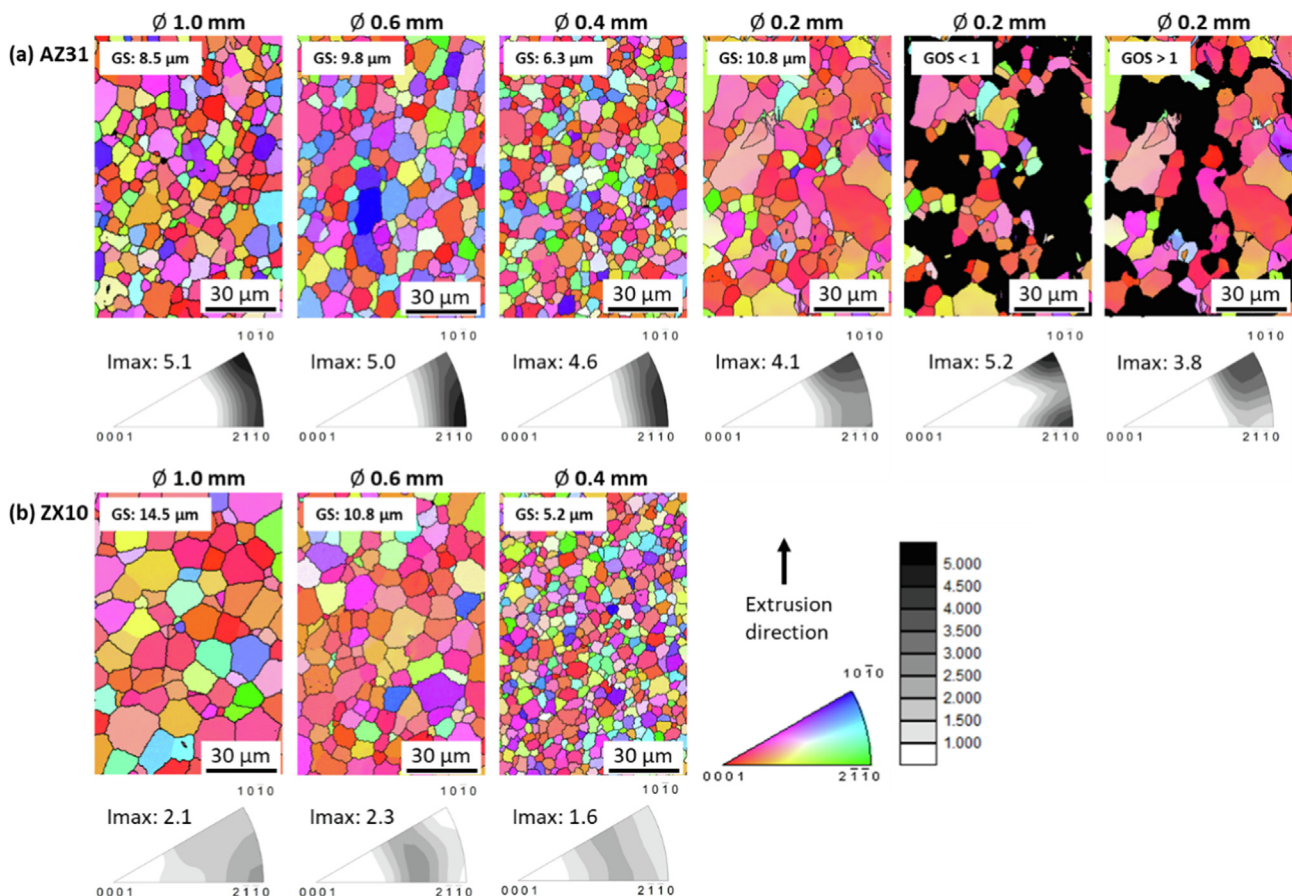
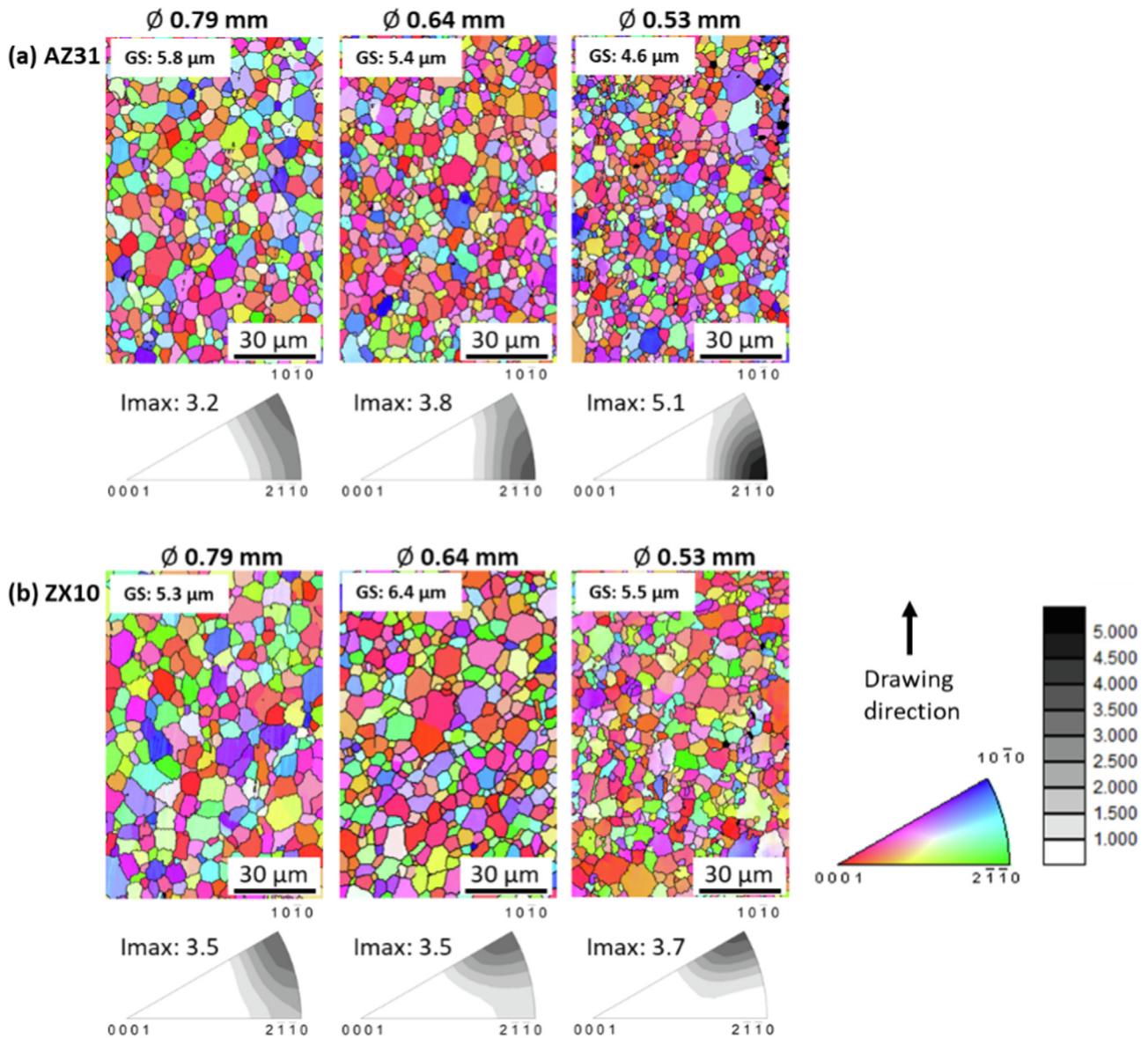


Fig. 1. Orientation maps from EBSD measurements on longitudinal section of the as extruded wires (extrusion direction (ED) vertical) and the corresponding inverse pole figures in the extrusion direction (ED) for (a) AZ31 and (b) ZX10.



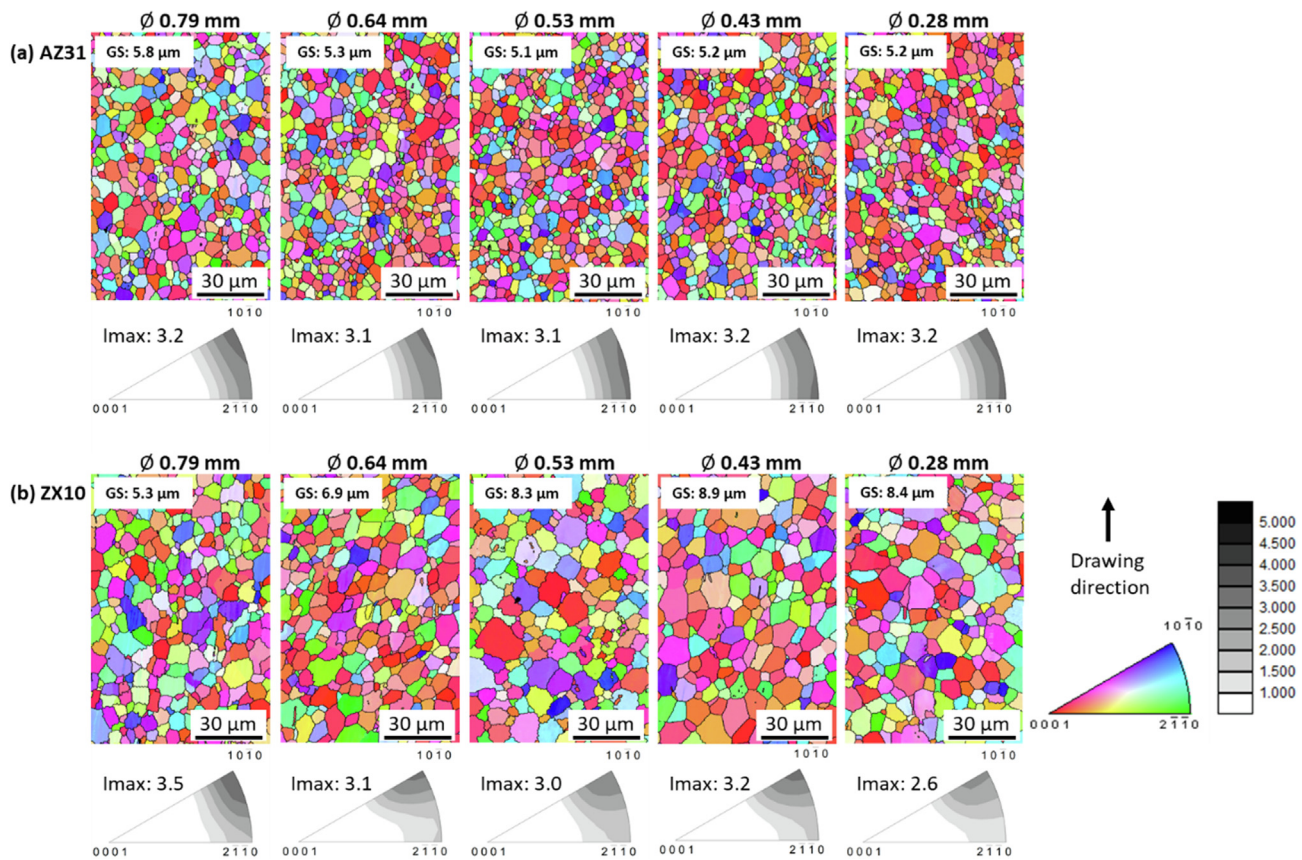
**Fig. 2.** Orientation maps from EBSD measurements on longitudinal section of the drawn wires according route 1 and the corresponding inverse pole figures in the drawing direction (DD) for (a) AZ31 and (b) ZX10.

tained basically without variations. In particular, no indication of the above-mentioned development of the “RE texture” of this alloy was found.

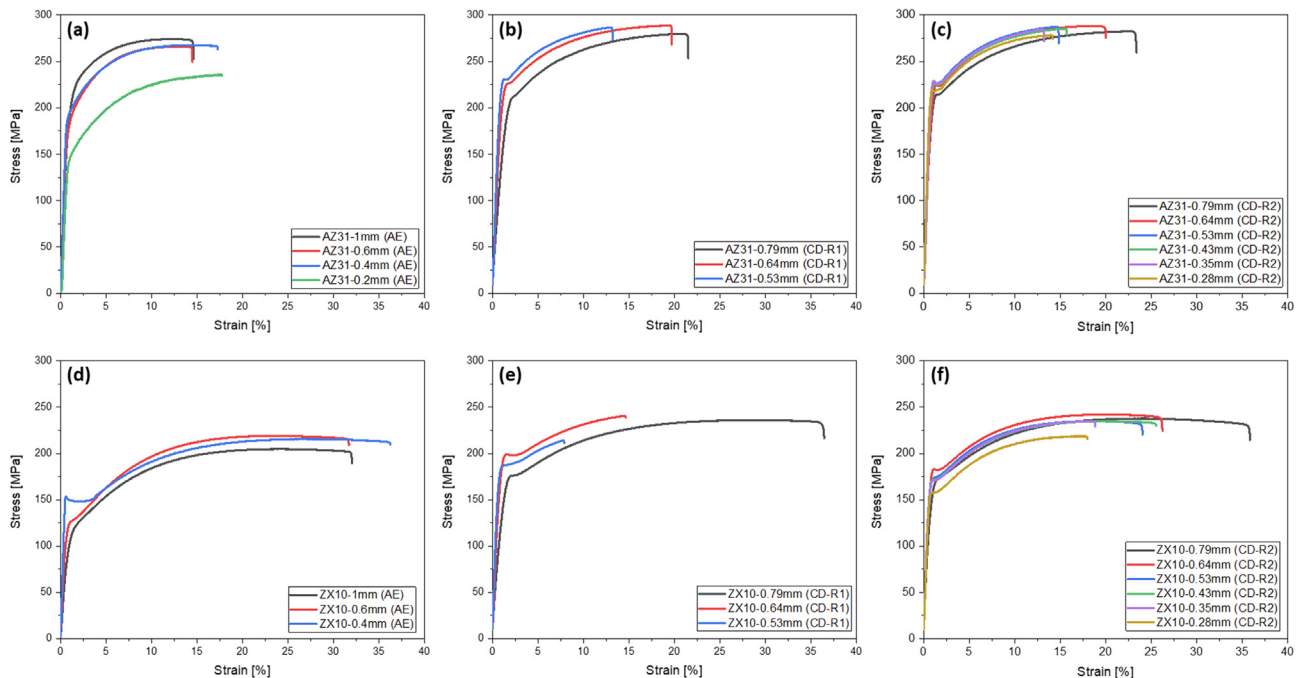
A variation of the cold drawing schedule includes the mentioned heat treatment of 5 min at 350 °C after each two cold-drawing passes before continuation for route 2. Fig. 3 shows the resulting microstructures and textures from EBSD measurements. A maximum of 12 passes has been applied following this schedule without reaching a processing limit for both alloys. While the grain structure for the AZ31 wires is fully recrystallized at comparable grain sizes as with the previous setup (route 1), weaker textures are obtained preferentially, at lower wire diameter, with distributed intensity along the arc between the  $\langle 10\text{--}10 \rangle$ - and  $\langle 11\text{--}20 \rangle$  poles. For ZX10, a slight increase in the average grain size is observed with increasing number of passes. Although no development of a previously reported recrystallization texture is observed with this processing setup either, a weakening of the dominating  $\langle 10\text{--}10 \rangle$  fibre texture with increasing number of passes, from 0.79 mm to 0.28 mm diameter, is observed.

Fig. 4 collects stress–strain diagrams of the as-extruded and drawn wires of various thicknesses. Table 3, Table 4 and Table 5 provide the corresponding mechanical parameters. In case of as extruded AZ31 wire (Fig. 4a), a continuous elasto-plastic transition leads into a typical strain hardening range with decreasing curve slope up to a stress maximum, which typically does not reveal a following stress drop due to necking. The strain hardening rate appears to be highest for the 1 mm wire, where the highest stress levels are also achieved, while it is lowest for the 0.2 mm wire, where the lowest stress levels are achieved as well. The as extruded ZX10 wires in Fig. 4d show a slight tendency of an S-shaped hardening range instead. In the literature there are several sources that prove that for textured Mg alloys, such hardening behaviour has often been associated with a preferential activation of twinning [51–53], which is likely active due to available grains with preferential orientation for twinning. The thinnest wire with 0.4 mm thickness reveals a very pronounced elastic limit indicating instable material flow (which could also be related to twinning) around yielding [54–56].





**Fig. 3.** Orientation maps from EBSD measurements on longitudinal section of the drawn wires according route 2 and the corresponding inverse pole figures in the DD for (a) AZ31 and (b) ZX10.



**Fig. 4.** Stress-strain diagram in ED from the wires (a) as extruded AZ31, (b) drawn Route 1 AZ31, (c) drawn route 2 AZ31; (d) as extruded ZX10, (e) drawn route 1 ZX10 and (f) drawn route 2 ZX10.

Wires from the two cold-drawing routes show generally a sharper yield point or even a pronounced elastic limit if the total degree of deformation was high as shown in Fig. 4b,c,e,f. This indicates the

initial remain of the strain hardening that the wires received during cold-drawing and is obviously related to the non-varied heat treatment applied. For both alloys after applying drawing route 1

**Table 3**

Mechanical properties from tension tests parallel to ED of the as extruded wires (tensile yield stress (TYS), ultimate tensile stress (UTS)) with standard deviations.

| As extruded (AE) | TYS [MPa] | UTS [MPa] | Fracture Strain [%] |
|------------------|-----------|-----------|---------------------|
| AZ31-1.0 mm      | 207 ± 1   | 277 ± 3   | 13.7 ± 0.3          |
| AZ31-0.6 mm      | 190 ± 1   | 267 ± 1   | 13.6 ± 0.4          |
| AZ31-0.4 mm      | 191 ± 1   | 269 ± 1   | 16.8 ± 0.4          |
| AZ31-0.2 mm      | 145 ± 1   | 234 ± 2   | 15.8 ± 1.9          |
| ZX10-1.0 mm      | 112 ± 1   | 204 ± 1   | 29.5 ± 1.3          |
| ZX10-0.6 mm      | 122 ± 1   | 220 ± 1   | 30.4 ± 0.7          |
| ZX10-0.4 mm      | 154 ± 2   | 217 ± 1   | 34.3 ± 1.2          |

**Table 4**

Mechanical properties from tension tests parallel to DD of the drawn wires according route 1 (tensile yield stress (TYS), ultimate tensile stress (UTS)) with standard deviations.

| Cold drawn route 1 (CD-R1) | TYS [MPa] | UTS [MPa] | Fracture Strain [%] |
|----------------------------|-----------|-----------|---------------------|
| AZ31-0.79 mm               | 203 ± 2   | 281 ± 1   | 21.9 ± 3.4          |
| AZ31-0.64 mm               | 209 ± 2   | 290 ± 2   | 19.7 ± 2.6          |
| AZ31-0.53 mm               | 219 ± 3   | 277 ± 13  | 9.1 ± 4.4           |
| ZX10-0.79 mm               | 169 ± 3   | 238 ± 1   | 34.1 ± 2.7          |
| ZX10-0.64 mm               | 189 ± 3   | 240 ± 1   | 13.8 ± 0.6          |
| ZX10-0.53 mm               | 187 ± 5   | 219 ± 11  | 7.4 ± 2.7           |

(AZ31 in Fig. 4b and ZX10 in Fig. 4e), the most significant effect is the reduced ductility with decreasing wire diameter. If intermediate heat treatment of the drawn wires is applied following drawing route 2, the variation of the reached stress levels is rather low for both alloys, see Fig. 4c, f. Thus, the mechanical properties are basically maintained despite the different total degree of forming. However, despite the intermediate heat treatment, there is a tendency for the fracture strain to decrease with increasing number of drawing passes.

Fig. 5 collects the mechanical properties for the different wire diameters for a more direct comparison. While the TYS and UTS and fracture strain for the AZ31 wires do not vary much (with the exception of the special condition of the 0.2 mm wire), somewhat higher TYS and UTS are observed for the two cold drawing routes. The TYS increases with decreasing wire diameter, which is not much seen for the UTS. Also, the annealed conditions of these wires are quite comparable after the two varied drawing routes. Interestingly, a higher fracture strain compared to the original extruded wires is found after the first drawing passes, which then decreases with further forming passes. Very similar findings are observed for ZX10 where the change of the fracture strain is much more distinct. Higher TYS and UTS for the thinnest wire are associated with the clearly finer grain structure of the material as recalled from Table 2.

**Table 5**

Mechanical properties from tension tests parallel to DD of the drawn wires according route 2 (tensile yield stress (TYS), ultimate tensile stress (UTS)) with standard deviations.

| Cold drawn route 2 (CD-R2) | TYS [MPa] | UTS [MPa] | Fracture Strain [%] |
|----------------------------|-----------|-----------|---------------------|
| AZ31-0.79 mm               | 203 ± 2   | 281 ± 1   | 21.9 ± 3.4          |
| AZ31-0.64 mm               | 213 ± 4   | 288 ± 1   | 19.2 ± 1.1          |
| AZ31-0.53 mm               | 221 ± 5   | 286 ± 2   | 14.2 ± 0.4          |
| AZ31-0.43 mm               | 218 ± 1   | 285 ± 1   | 16.1 ± 3.1          |
| AZ31-0.35 mm               | 225 ± 1   | 286 ± 2   | 13.5 ± 2.5          |
| AZ31-0.28 mm               | 218 ± 1   | 278 ± 2   | 13.8 ± 2.8          |
| ZX10-0.79 mm               | 169 ± 3   | 238 ± 1   | 34.1 ± 2.7          |
| ZX10-0.64 mm               | 180 ± 3   | 241 ± 1   | 25.3 ± 1.3          |
| ZX10-0.53 mm               | 172 ± 2   | 234 ± 1   | 22.1 ± 7.9          |
| ZX10-0.43 mm               | 169 ± 1   | 235 ± 1   | 24.2 ± 0.6          |
| ZX10-0.35 mm               | 170 ± 2   | 235 ± 1   | 19.1 ± 1.9          |
| ZX10-0.28 mm               | 160 ± 2   | 222 ± 3   | 18.4 ± 4.3          |

Fig. 6a-d show exemplary images of the wire surface in order to image the different surface structures after extrusion and after wire drawing and in Fig. 6e the resulting mean arithmetic height ( $S_a$ ) as a determination of the surface roughness is plotted. While the surface quality itself is directly influenced by the inner die surfaces and therefore may not continuously vary with the wire diameter, it is remarkable that extruded AZ31 wire (black colour) show a distinctly higher roughness compared to extruded ZX10 wire, indicating more homogeneous forming of the latter alloy. No such alloy-specific difference is found for cold drawing route 1 (red colour), and the opposite finding for wire drawing route 2 (blue colour) is also not strongly pronounced. However, the roughness increases with decreasing wire diameter in the cold drawing cases, which could also be due to poorer machined drawing dies at smaller diameters. Note that drawn wires generally appear with lower roughness compared to their extruded counterparts.

Fig. 7 collects images of the wires after the knot test and the corresponding stress ratios in the form of the ratio between the fracture stress during the knot test in relation to the UTS. It can be seen that there is a clear difference between the alloys and the manufacturing processes. For the extruded wires, a constant stress ratio of around 0.55 is seen for all AZ31 experiments, except for the 0.2 mm wire (partially recrystallized microstructure). Due to the inhomogeneous microstructure, there is a significant decrease in the stress ratio for the 0.2 mm AZ31 wires. In comparison, the extruded ZX10 wires show a significant increase in the stress ratio with thinner wires and consequently a decrease of the texture intensity and formation of the rE-component. For the drawn wires after route 1, it can also be seen that with increasing deformation (and decreasing elongation at fracture), the stress ratio decreases significantly. This is particularly evident for the 0.53 mm ZX10 wire (6x 20 % reduction). This wire is the only one to show premature failing during the knot test. The drawn wires according to route 2 tend to higher stress ratios than those according to route 1, whereas the comparison of AZ31 and ZX10 wires show different behaviours compared to the extruded ones: e.g. for AZ31, the as-extruded wires always have the lowest stress ratio and the as-extruded ZX10 wires the highest stress ratios. The same correlations could already be seen for the texture intensity.

#### 4. Discussion

To compare the influence of the process on the wire properties, it is important to consider the recrystallization mechanisms. Depending on the process, DRX dominates in extrusion and SRX dominates in wire drawing and therefore the texture and microstructure development. In a previous work [26] on wire extrusion, it has already been shown that the results of the wires indicate a strong correlation with the extrusion of round bars, which is basically understood as the same shape giving approach at lower **degrees of deformation**. Therefore, the results from the extruded wires are correlated with the literature from extruded bars. Looking at the **microstructure** and **texture development** during cold drawing of wires, correlations to the rolling process can be seen due to the prevailing recrystallization mechanism. Thus, these results are compared with those of rolled flat products by means of a pronounced SRX. As for the **mechanical properties**, the **crystallographic orientation** of the grains and their influence are considered.

It is noteworthy, that processing of wires in this study has been realized by applying forming schedules with relatively **high degrees of deformation** for a class of material, which is often associated with limited formability due to the hexagonal close packed lattice structure [57]. Even though the used extrusion setup is not of the size of a typical industrial extrusion press for profile produc-



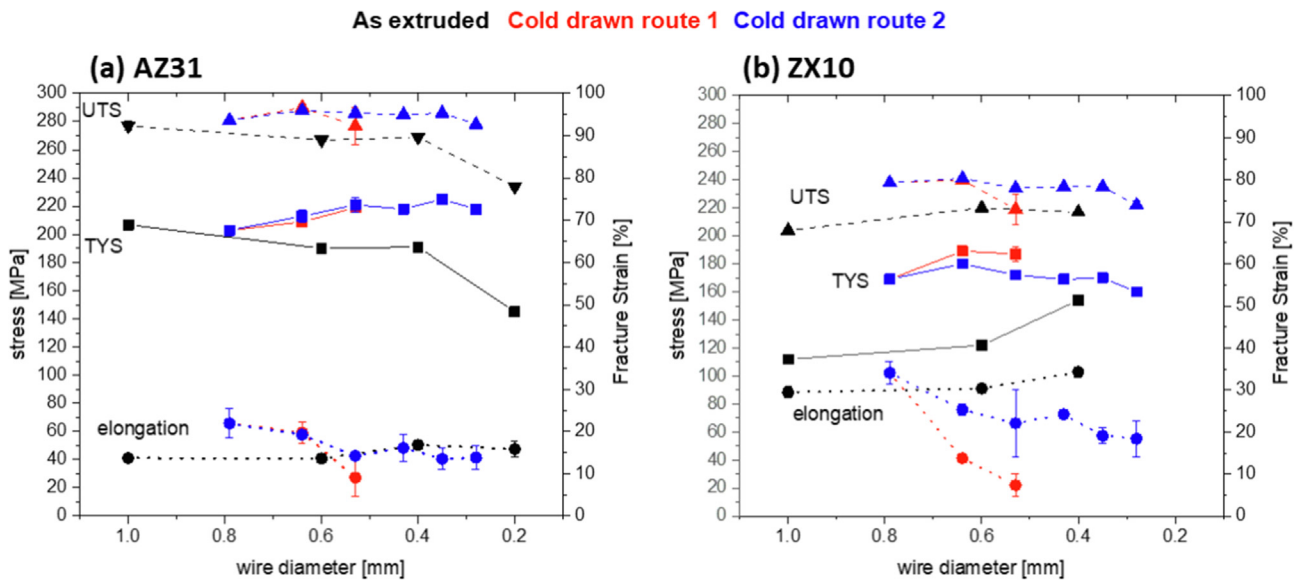


Fig. 5. Mechanical properties of the wires for various wire diameter for (a) AZ31 and (b) ZX10.

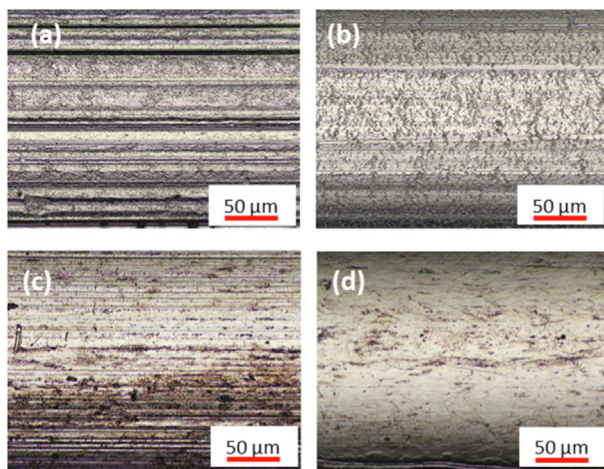
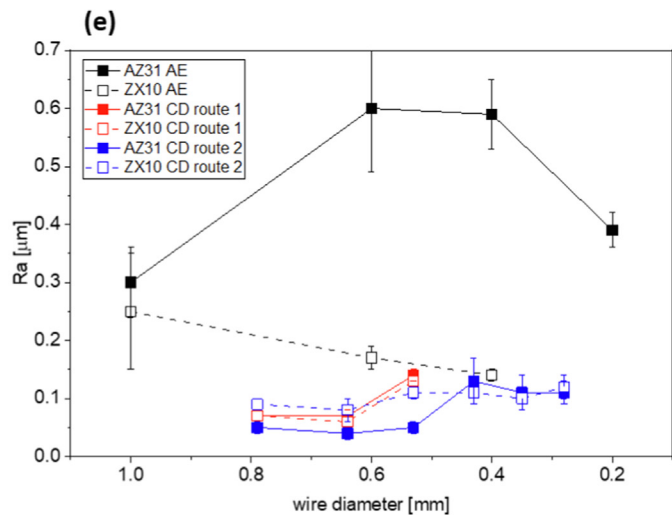


Fig. 6. Exemplary images of the wire surface for (a) AZ31 as extruded 0.6 mm, (b) ZX10 as extruded 0.6 mm, (c) AZ31 drawn route 2 0.64 mm, (d) ZX10 drawn route 2 0.64 mm and (e) shows the averaged surface roughness ( $S_a$ ) in  $\mu\text{m}$  vs wire diameter in mm for all wires.



tion, it has a very good specific pressure (with a force limit of 2.5 MN related to the punch diameter of 50 mm) for the manufacturing of products such as wires or feedstock material for implant manufacturing and can achieve high degrees of deformation, like in this study. Still, limitations may apply if alloys are suggested, which are less formable compared to the rather dilute alloys of this study, AZ31 and ZX10.

As shown in Table 2, in this study, the forming of wires with a diameter of 0.4 mm is feasible with the fourfold setup described above. The microstructure development is very comparable to those of round bar extrusions. Furthermore, degrees of deformation during the cold drawing schedules are also very high in an attempt to enhance the associated cold-forming microstructure development. Compared to cold drawing with subsequent heat treatment, where SRX dominates texture and microstructure development, the very high degree of deformation in extrusion leads to significant DRX during the forming process. As many recent researches have shown [58–61], the main influence on the kinetics of this DRX can be attributed to temperature and strain

rate, which is often represented in terms of the Zener-Hollomon parameter, a temperature-compensated strain rate. The influence of the applied strain due to the extrusion ratio enters indirectly as the strain rate - seen as the extrusion exit speed - which results from a constant extrusion die speed. It increases with increasing extrusion ratio. Moreover, a higher strain rate during extrusion leads to higher deformation-induced heating, which increases the relevant temperature for DRX [39,47,62]. It should be noted that as the extrusion ratio increases, the wire diameter decreases, resulting in a faster cooling rate, which is in contrast to the acceleration of recrystallization and thus grain growth at higher extrusion ratios.

These findings correlate with the **microstructure development** of the extruded wires for AZ31 and ZX10 (see Fig. 1). For the as extruded AZ31 wires (1.0 mm to 0.4 mm), the average grain size shows only a very small variation. The exit velocity is approximately constant (8.7 to 9.8 m/min) as a function of wire diameter. The 0.4 mm wire has smaller grain size, here the higher cooling rate with smaller wire diameter seems to inhibit grain growth. This

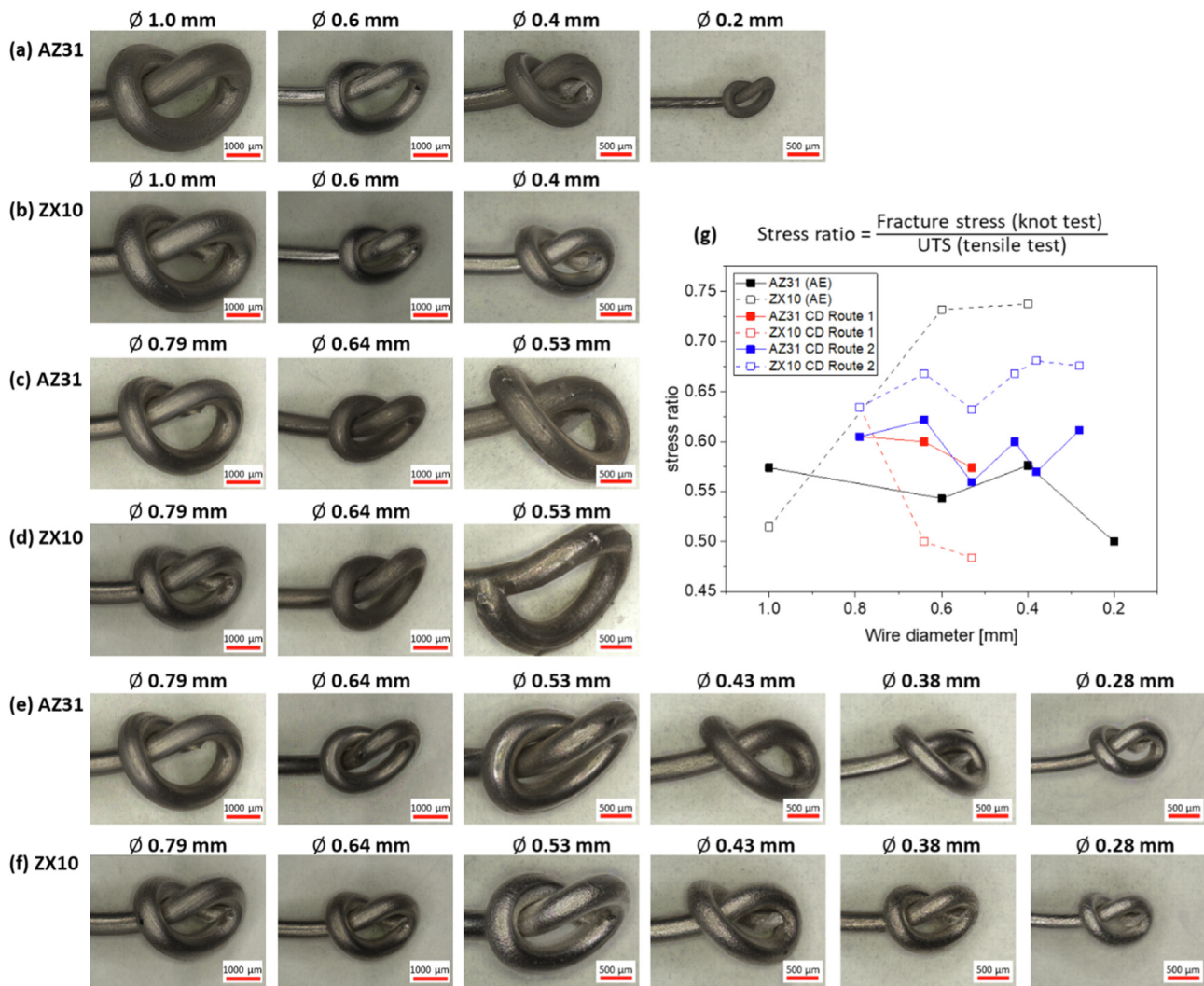


Fig. 7. Images of the wires after the knot test for alloys AZ31 and ZX10 (a, b) as extruded; (c, d) cold drawn route 1; (e, f) cold drawn route 2; (g) corresponding stress ratios.

results in a smaller grain size, despite a higher degree of deformation, with a lower wire diameter. For the ZX10 wires (1.0 mm to 0.6 mm), in contrast to the AZ31 wires, there is a significant decrease in exit velocity (6.0 to 3.7 m/min), which is clearly reflected in a small grain size with a smaller wire diameter. For the 0.6 mm and 0.4 mm ZX10 wires, the exit velocity is almost the same. As for the AZ31 wire, the smaller wire diameter leads to faster cooling and thus to a smaller grain size. An exception is the 0.2 mm AZ31 wire (Fig. 1 a): despite the extremely high degree of deformation, this wire is the only one with a partly recrystallized microstructure. It is important to note that this wire was processed at the process limit, which also results in the lowest exit velocity. This very low exit velocity means that the forming heat during the process is not sufficient to recrystallize the microstructure completely.

As in case of the extruded wires, the drawn wires (Fig. 2 and Fig. 3) also present a grain size dependence after subsequent heat treatment (SRX) on the wire diameter and the applied wire drawing route. Compared to the extruded wires the variation is not as large, but the thinner wire diameter and the higher degree of deformation are, the main reasons for the differences in grain size. As shown in route 1 for AZ31 (Fig. 2), a higher degree of deformation (higher dislocation density) leads to a higher nucleation rate, resulting in a finer-grained microstructure for the 0.53 mm wire compared to

the 0.79 mm wire. In contrast, the ZX10 wire (route 1) does not exhibit significant grain size development. The average grain size varies between 5.3 and 6.4  $\mu\text{m}$ . The reason for this could be that the number of defects, with increasing degree of deformation, change less in the ZX10 wire than in the AZ31 wire. This leads to a lower nucleation density and thus to a lower variation in grain size. The grain size development for the wires according to route 2 (Fig. 3) does not reveal a large variation for AZ31. For ZX10, on the other hand, there is a slight increase in grain size with small wire diameter. Even for the extruded wire, ZX10 exhibits a larger grain size, as a function of wire diameter. This indicates a clear difference in the static as well as dynamic recrystallization mechanisms for ZX10 and AZ31. It is known that the recrystallization behaviour depends on the mechanism (SRX, DRX) [14,18] and the alloy [15,16].

The influence of the alloy and the recrystallization mechanisms becomes much clearer considering **texture development** as a function of the manufacturing process (extrusion or drawing). As already mentioned, the DRX dominates the microstructure and texture development of the wires during extrusion and the SRX during cold drawing with subsequent heat treatment.

For AZ31 wires, the texture components known from the literature are found in the extruded as well as in the drawn wires [15,47,49,63]. Typically for extruded rods and also the AZ31 wires, there is a clear preference for the orientation of the basal planes

parallel to the ED. For the as extruded wires (Fig. 1 a) the 1.0 to 0.4 mm diameter wire a double-fibre along the arc between the  $\langle 10\text{--}10 \rangle$ - and the  $\langle 11\text{--}20 \rangle$ -poles dominates the texture, which is typical for recrystallized extruded rods [64]. Whereas the 0.2 mm wire, shows a strong prismatic fibre with high intensity in the  $\langle 10\text{--}10 \rangle$  pole. This has been often associated with the remains of strong deformation textures in essentially all magnesium alloy extrusions [49,65,66] and also fits with the results in this study. After GOS separation (Fig. 1) the non-recrystallized microstructure exhibits a  $\langle 10\text{--}10 \rangle$  fibre component and the recrystallized microstructure also has a  $\langle 11\text{--}20 \rangle$  fibre component. The recrystallization leads to a tilt component with a rotation of up to  $30^\circ$  around the c-axis [49]. The drawing process for the AZ31 wires (Fig. 2, Fig. 3), i.e. the SRX, leads to no change in the texture components. Compared to extrusion, i.e. DRX, there is a different appearance of the components depending on the wire drawing route and thus the degree of deformation. route 1 clearly shows that higher deformation leads to a more pronounced shaping of the  $\langle 11\text{--}20 \rangle$  fibre. This means that a higher dislocation density leads to the development of more grains with the recrystallization component during SRX. It is also reported that an excessively high degree of deformation, like in case of the wire drawing according route 1, as a result of a lower rolling temperature or a high extrusion ratio, leads to an increase in texture intensity after additional heat treatment [62,67]. Due to the many intermediate annealing in route 2, texture weakening occurs with a double fibre along the arc between the  $\langle 10\text{--}10 \rangle$  and the  $\langle 2\text{--}1\text{--}10 \rangle$  poles, which is also typical for extruded rods [64]. Bohlen et al. [19] show for AZ31 that rolled sheets (i.e. massive cold forming with subsequent heat treatment) tend to have a lower texture intensity than extruded profiles. Thus, in the case of AZ31 wires, DRX seems to lead to a higher texture intensity than SRX (in case of route 2, see Fig. 3).

For the ZX10 wires, more variation in texture components is shown as a function of the manufacturing process. It is generally known, that the use of RE or Ca leads to a component that is concentrated with high intensity in the  $\langle 2\text{--}1\text{--}10 \rangle$  pole, resulting in a tilt of the basal planes out of the ED. The delay in recrystallization and the corresponding new orientations of the grains also include an influence of twins and shear bands on the new grain orientation [68–71]. For the as extruded ZX10 wires (Fig. 1 b), the 1 mm wire shows a very weak  $\langle 11\text{--}20 \rangle$  fibre component and with decreasing wire diameter the “RE texture component” clearly appears. Whereas for the drawn wires (Fig. 2 (route 1) and Fig. 3 (route 2)) the  $\langle 11\text{--}20 \rangle$  fibre component dominates the texture without any tilts of basal planes out of the extrusion direction. Thus, there is a clear influence of the recrystallization mechanism on texture development. Only during DRX (extrusion) it is possible to develop the RE texture component in ZX10 wires. Cano et al. [15] show for extruded 10 mm ZX10 bars that the type of recrystallization is crucial for texture development. By heat treating partially recrystallized microstructures, i.e. SRX, it was shown that the  $\langle 10\text{--}10 \rangle$  fibre component dominates the texture here as well. Whereas with increasing extrusion speed, i.e. DRX, the  $\langle 10\text{--}10 \rangle$  fibre component disappears and the RE component prevails. This texture evolution, due to SRX, is consistent with that of cold-drawn heat-treated wires, as the  $\langle 10\text{--}10 \rangle$  fibre component dominates the texture regardless of the wire drawing route. In the as extruded ZX10 wires, there is a development with decreasing wire diameter from  $\langle 11\text{--}20 \rangle$  component to the RE texture component. Dobron et al. [50] suggested that at higher extrusion temperatures the RE texture disappears and  $\langle 10\text{--}10 \rangle$ - $\langle 21\text{--}1\text{--}0 \rangle$  fibre forms by recrystallization. Therefore, correlating with the results from this study (Fig. 1), it can be assumed that due to the larger grain size (higher exit velocity and so higher deformation temperature) of the 1 mm ZX10 wire, that recrystallization is more advanced in this wire and thus the RE component does not dominate the texture. In terms of

texture intensities, an increase in maximum intensity can be observed for the ZX10 wires due to cold drawing compared to the extruded conditions. AZ31 wires exhibited an opposite behaviour: In correlation with the grain size, a decrease of the texture intensity with the grain growth can be observed. A similar behaviour has already been observed for pure magnesium [72].

As in the case of texture and microstructure development, it is also evident from the mechanical properties that both the manufacturing process and the alloy composition have an influence. It is known that the **crystallographic orientation** of the grains is the main factor influencing the **mechanical properties** [43,73–75].

Tensile tests were performed to investigate the uniaxial stress case and the knot test (see Fig. 7), which tends to represent the application case, offers the opportunity to represent a biaxial stress case. In Nienaber et al. [26] it was already shown by means of a wrapping test that different stress states (compression and tension) act on the material. Geometrically, the wrapping test is similar to the knot test. Consequently, it also offers the possibility of making a statement about the biaxial formability. To quantify the results, the stress ratio was calculated from the TYS and the stress failure (knot test). Hence, a 1 means that there is no difference in stress absorption between the uniaxial and biaxial stress cases. It is known from the literature that a weak quadrupole texture is required in flat products for high biaxial deformability to allow basal sliding from all directions [16,76]. In the case of round profiles, the compression-tension asymmetry is considered [15,47,63].

For the as extruded AZ31 wires, a strong alignment of the basal planes along the  $\langle 10\text{--}10 \rangle$  and  $\langle 21\text{--}1\text{--}0 \rangle$  poles is shown. In this case, the ability to activate basal slip is lower in both stress cases, uniaxial (tensile test) and biaxial (knot test). Therefore, the stress properties remain comparatively high and the strain levels low, because the strain hardening capability of the specimen is limited (see Fig. 4 a). Due to the drawing process, although the texture components in AZ31 wires do not change significantly, there is a weakening of the texture intensity, which can justify the primary increase in ductility (independent on the drawing route) up to a wire diameter of 0.64 mm (see Fig. 4 b, c). From smaller wire diameters on, the ductility decrease again, as summarized in Fig. 5a. The decrease in ductility occurs simultaneously with the increase in surface roughness (see Fig. 6e). It can be assumed that with an increase of the number of drawing steps, the defects in the surface and in the material become larger (and can no longer be annealed out) and thus ductility decreases. The AZ31 wires also show differences in strength depending on the manufacturing process. The drawing process results in a significant increase in UTS and TYS with decreasing wire diameter. It is known that the strength of metals generally increases with decreasing grain size due to grain boundary hardening. An indication of the onset of plastic yielding is the yield strength, since it is determined by the effect of dislocation mobility in a polycrystalline material. As the number of grain boundaries increases, the transition of dislocation activity between grains becomes more difficult and higher stresses are required. This relationship of the yield strength to grain size dependence is explained by the Hall-Petch relationship [77,78]. This finding is consistent with grain refinement by the drawing process and the associated increase in strength of AZ31 wires. With regard to the knot test (biaxial ductility), AZ31 also shows an influence of the manufacturing process (but not as pronounced as for ZX10). Similar to the ductility, there is a significant improvement of the stress ratio by the first drawing step. After that, the stress ratio decreases. Once again, the relationship with texture decrease and surface roughness increase can be associated.

For the ZX10 wires, a very similar trend in the mechanical properties, as shown in Fig. 5b, can be observed as a result of the manufacturing process. In this case, the increase in strength is not only due to the grain size (Hall-Petch), but also due to a change in the



texture caused by the drawing process (SRX). During wire drawing of ZX10, the rE-texture component disappears and a  $<10\text{--}10>$  fibre component appears. This component makes basal sliding more difficult and thus leads to an increase in UTS and TYS. In the case of the rE-texture component, basal planes are tilted out the ED, the slip activation in the uniaxial case is enhanced and the ability to adapt to the load is increased [79,80]. Whereby the elongation increases, but at the same time the yield strength decreases, as shown in Fig. 5b. This basal plane deflection is shown in the extruded 0.4 mm and 0.6 mm wires (see Fig. 1b). In terms of grain size, the 0.4 mm wire is among the finest with a grain size of 5.2  $\mu\text{m}$ , but has a lower TYS than the drawn wires with higher grain size. But the drawn wires also have a higher texture intensity and so a restriction of the basal slip leads to a strengthening of the material. Regarding the ductility of the ZX10 wires, it can also be seen that there is an increase by applying the first drawing step (2x 20 % reduction). In correlation with the texture, this behaviour is difficult to explain, since the extruded 0.6 mm and 0.4 mm wires have a better texture (tilt of basal planes out of ED and low intensity) to activation of basal slip [75,81,82]. Again, this behaviour can be explained by a significant improvement in the surface roughness due to the wire drawing process. Overall, the texture has a significant influence. Similar to flat products, a weak texture with a rE-component leads to a low compression-tension asymmetry in round bars. This same behaviour can be observed in the knot test (see Fig. 7g). The lower the texture intensity, the higher the stress ratio. In addition, the tilt of the basal plane (ZX10 as-extruded 0.6 mm and 0.4 mm wires) allows the material to reach a maximum stress ratio close to 0.75.

## 5. Conclusion

The aim of this work was to investigate and understand the impact of the wire manufacturing process on the mechanical property development of two magnesium alloys, AZ31 and ZX10. To achieve this, wires were manufactured along two processing routes (direct extrusion and cold wire drawing with heat treatment) to allow direct comparison of the alloy dependent influence on the microstructure and texture development and therefore on the mechanical properties.

During this work, the following main results were obtained:

- Direct extrusion of wires with a high extrusion rate of up to 1:15625 were possible, resulting in wires with 0.2 mm (AZ31), respectively 0.4 mm (ZX10) diameter, while the limit of the cold drawing routes were strongly influenced by the use of heat treatments.
- It was shown that DRX is the dominant mechanism for texture development in extrusion and SRX in wire drawing, resulting in different textures and property profiles.
- Regarding the mechanical properties, it was demonstrated, that they are mainly influenced by the texture and the texture development in turn depends on the manufacturing process, the wire diameter and the alloy composition.
- It is possible to improve the properties significantly by drawing. There is however only a small window (diameter reduction) to improve the properties compared to the as-extruded wires.
- In relation to an application of wires, the stress factor is a very important value. It indicates how much strength the wire loses before it breaks due to the biaxial load. This work shows that the extruded ZX10 wires have the greatest application potential (highest stress factor). Although the one-time drawn wires show a higher elongation in comparison, the advantageous texture due to the DRX during extrusion prevails for the extruded ZX10 wires.

## Data availability

The raw/processed data required to reproduce these findings cannot be shared at this time as the data also forms part of an ongoing study.

## Author contributions

Experimental works were carried out by MN and MB with continuous discussion with JB and NBK. All authors discussed the experimental results and the conclusion and contributed to writing the submitted manuscript.

## Funding

This research did not receive any specific grant from funding agencies in the public, commercial, or not-for-profit sectors.

## Data availability

Data will be made available on request.

## Declaration of Competing Interest

The authors declare that they have no known competing financial interests or personal relationships that could have appeared to influence the work reported in this paper.

## Acknowledgements

The authors would like to thank Mr. Günther Meister and Mr. Alexander Reichart for their help during casting and machining of the billets.

## References

- [1] D. Mei, C. Wang, M. Nienaber, M. Pacheco, A. Barros, S. Neves, R.L. Reis, S. Zhu, J. Bohlén, D. Letzig, et al., Corrosion behavior of Mg wires for ureteral stent in artificial urine solution, *Corros. Sci.* 189 (2021), <https://doi.org/10.1016/j.corsci.2021.109567>.
- [2] He, X.; Li, Y.; Miao, H.; Sun, J.; Ong, M.T.Y.; Zu, H.; Li, W. The Bioactive Mg-Zn-Gd Wire Enhances Musculoskeletal Regeneration: An In Vitro Study. *Crystals* 2022, 12, 10.3390/cryst12091287.
- [3] D. Xia, F. Yang, Y. Zheng, Y. Liu, Y. Zhou, Research status of biodegradable metals designed for oral and maxillofacial applications: A review, *Bioact. Mater.* 6 (2021) 4186–4208, <https://doi.org/10.1016/j.bioactmat.2021.01.011>.
- [4] F. Witte, N. Hort, C. Vogt, S. Cohen, K.U. Kainer, R. Willumeit, F. Feyerabend, Degradable biomaterials based on magnesium corrosion, *Curr. Opin. Solid State Mater. Sci.* 12 (2008) 63–72, <https://doi.org/10.1016/j.cossms.2009.04.001>.
- [5] A. Milenin, P. Kustra, D. Byrska-Wójcik, M. Wróbel, M. Pačko, J. Sulej-Chojnacka, S. Matuszyńska, B. Płonka, The effect of in vitro corrosion on the mechanical properties of metallic high strength biodegradable surgical threads, *Arch. Civil Mech. Eng.* 20 (2020), <https://doi.org/10.1007/s43452-020-00062-w>.
- [6] A. Milenin, P. Kustra, J.-M. Seitz, F.-W. Bach, D. Bormann, Production of thin wires of magnesium alloys for surgical applications, *Wire J. Int.* (2011) 64–71.
- [7] J.E. Bergsma, F.R. Rozema, R.R.M. Bos, G. Boering, W.C. de Bruijn, Late degradation tissue response to poly(L-lactide) bone plates and screws, in: D. F. Williams (Ed.), *The Biomaterials: Silver Jubilee Compendium*, Elsevier Science, Oxford, 1995, pp. 101–107.
- [8] A. Milenin, M. Wróbel, P. Kustra, M. Packo, D. Byrska-Wójcik, J. Sulej-Chojnacka, B. Płonka, Mechanical properties, crystallographic texture, and in vitro bio-corrosion of low-alloyed Zn-Mg, produced by hot and cold drawing for biodegradable surgical wires, *Arch. Civil Mech. Eng.* 21 (2021), <https://doi.org/10.1007/s43452-021-00311-6>.
- [9] Chen, J.; Tan, L.; Yu, X.; Etim, I.P.; Ibrahim, M.; Yang, K. Mechanical properties of magnesium alloys for medical application: A review. *Journal of the Mechanical Behavior of Biomedical Materials* 2018, 87, 68–79, <https://doi.org/10.1016/j.jmbbm.2018.07.022>.
- [10] J. Hirsch, T. Al-Samman, Superior light metals by texture engineering: Optimized aluminum and magnesium alloys for automotive applications, *Acta Mater.* 61 (2013) 818–843, <https://doi.org/10.1016/j.actamat.2012.10.044>.

- [11] W.J. Joost, P.E. Krajewski, Towards magnesium alloys for high-volume automotive applications, *Scr. Mater.* 128 (2017) 107–112, <https://doi.org/10.1016/j.scriptamat.2016.07.035>.
- [12] R. Cottam, J. Robson, G. Lorimer, B. Davis, Dynamic recrystallization of Mg and Mg-Y alloys: Crystallographic texture development, *Mater. Sci. Eng., A* 485 (2008) 375–382, <https://doi.org/10.1016/j.msea.2007.08.016>.
- [13] M.G. Jiang, C. Xu, H. Yan, S.H. Lu, T. Nakata, C.S. Lao, R.S. Chen, S. Kamado, E.H. Han, Correlation between dynamic recrystallization and formation of rare earth texture in a Mg-Zn-Cd magnesium alloy during extrusion, *Sci. Rep.* 8 (2018) 16800, <https://doi.org/10.1038/s41598-018-35170-4>.
- [14] Nienaber, M.; Kurz, G.; Letzig, D.; Kainer, K.U.; Bohlen, J. Effect of Process Temperature on the Texture Evolution and Mechanical Properties of Rolled and Extruded AZ31 Flat Products. *Crystals* **2022**, 12, 10.3390/cryst12091307.
- [15] G. Cano-Castillo, J. Victoria-Hernandez, J. Bohlen, D. Letzig, K.U. Kainer, Effect of Ca and Nd on the microstructural development during dynamic and static recrystallization of indirectly extruded Mg-Zn based alloys, *Mater. Sci. Eng., A* 793 (2020), <https://doi.org/10.1016/j.msea.2020.139527>.
- [16] M. Nienaber, K.U. Kainer, D. Letzig, J. Bohlen, Processing Effects on the Formability of Extruded Flat Products of Magnesium Alloys, *Front. Mater.* 6 (2019), <https://doi.org/10.3389/fmats.2019.00253>.
- [17] Y. Li, P.J. Hou, Z.G. Wu, Z.L. Feng, Y. Ren, H. Choo, Dynamic recrystallization of a wrought magnesium alloy: Grain size and texture maps and their application for mechanical behavior predictions, *Mater. Des.* 202 (2021), <https://doi.org/10.1016/j.matdes.2021.109562>.
- [18] J. Victoria-Hernandez, S. Yi, D. Klumunzer, D. Letzig, Recrystallization behavior and its relationship with deformation mechanisms of a hot rolled Mg-Zn-Ca-Zr alloy, *Mater. Sci. Eng., A* 761 (2019), <https://doi.org/10.1016/j.msea.2019.138054>.
- [19] J. Bohlen, G. Cano, D. Drozdenco, P. Dobron, K.U. Kainer, S. Gall, S. Muller, D. Letzig, Processing Effects on the Formability of Magnesium Alloy Sheets, *Metals* 8 (2018) 147, <https://doi.org/10.3390/met8020147>.
- [20] P. Maier, A. Griebel, M. Jahn, M. Bechly, R. Menze, B. Bittner, J. Schaffer, Corrosion Bending Fatigue of RESOLVO<sup>®</sup> and WE43 Magnesium Alloy Wires, In *Magnesium Technology 2019: The Minerals, Metals & Materials Series* (2019) 175–181.
- [21] Sun, L.; Bai, J.; Xue, F.; Chu, C.; Meng, J. The Work Softening Behavior of Pure Mg Wire during Cold Drawing. *Materials (Basel)* **2018**, 11, 10.3390/ma11040602.
- [22] K. Yan, J.P. Sun, J. Bai, H. Liu, X. Huang, Z.Y. Jin, Y.N. Wu, Preparation of a high strength and high ductility Mg-6Zn alloy wire by combination of ECAP and hot drawing, *Materials Science and Engineering a-Structural Materials Properties Microstructure and Processing* 739 (2019) 513–518, <https://doi.org/10.1016/j.msea.2018.09.007>.
- [23] J.M. Seitz, D. Utermohlen, E. Wulf, C. Klose, F.W. Bach, The Manufacture of Resorbable Suture Material from Magnesium - Drawing and Stranding of Thin Wires, *Adv. Eng. Mater.* 13 (2011) 1087–1095, <https://doi.org/10.1002/adem.201100152>.
- [24] J. Eickemeyer, A. Güth, M. Falter, R. Opitz, Drawing of Magnesium Wires at Ambient Temperature. In *Magnesium* (2003) 318–323.
- [25] P. Kustra, A. Milenin, D. Byrka-Wojcik, O. Grydin, M. Schaper, The process of ultra-fine wire drawing for magnesium alloy with the guaranteed restoration of ductility between passes, *J. Mater. Process. Technol.* 247 (2017) 234–242, <https://doi.org/10.1016/j.jmatprotec.2017.04.022>.
- [26] M. Nienaber, S.B. Yi, K.U. Kainer, D. Letzig, J. Bohlen, On the Direct Extrusion of Magnesium Wires from Mg-Al-Zn Series Alloys, *Metals* 10 (2020) 1208, <https://doi.org/10.3390/met10091208>.
- [27] K. Tesar, K. Balik, Z. Sucharda, A. Jager, Direct extrusion of thin Mg wires for biomedical applications, *Trans. Nonferrous Metals Soc. China* 30 (2020) 373–381, [https://doi.org/10.1016/S1005-6326\(20\)65219-0](https://doi.org/10.1016/S1005-6326(20)65219-0).
- [28] J.M. Seitz, E. Wulf, P. Freytag, D. Bormann, F.W. Bach, The Manufacture of Resorbable Suture Material from Magnesium, *Adv. Eng. Mater.* 12 (2010) 1099–1105, <https://doi.org/10.1002/adem.201000191>.
- [29] A. Jager, S. Habr, K. Tesar, Twinning-detwinning assisted reversible plasticity in thin magnesium wires prepared by one-step direct extrusion, *Mater. Des.* 110 (2016) 895–902, <https://doi.org/10.1016/j.matdes.2016.08.016>.
- [30] Y. Zhang, J. Cao, M. Lu, Y. Shao, K. Jiang, X. Yang, X. Xiong, S. Wang, C. Chu, F. Xue, et al., A biodegradable magnesium surgical staple for colonic anastomosis: In vitro and in vivo evaluation, *Bioact Mater* 22 (2023) 225–238, <https://doi.org/10.1016/j.bioactmat.2022.09.023>.
- [31] S.H.A. Rizvi, C. Jiale, A. Mehboob, U. Zaheer, S.-H. Chang, Experimental study on magnesium wire-poly(lactic acid) biodegradable composite implants under in vitro material degradation and fatigue loading conditions, *Compos. Struct.* 272 (2021), <https://doi.org/10.1016/j.compstruct.2021.114267>.
- [32] H. Zhang, Y. Shen, Y. Ding, R. Li, J. Lei, In vitro corrosion and in vivo behavior of high strength Mg-6Zn-1Mn alloy wire for gastrointestinal anastomosis nail application, *Biomaterials, Advances* 142 (2022), <https://doi.org/10.1016/j.bioadv.2022.213159>.
- [33] M.B. Zheng, G.Q. Xu, D.B. Liu, Y. Zhao, B.Q. Ning, M.F. Chen, Study on the Microstructure, Mechanical Properties and Corrosion Behavior of Mg-Zn-Ca Alloy Wire for Biomaterial Application, *J. Mater. Eng. Perform.* 27 (2018) 1837–1846, <https://doi.org/10.1007/s11665-018-3278-x>.
- [34] M. Braatz, J. Bohlen, N. Ben Khalifa, Process Stability and Reproducibility of the Dieless Drawing Process for AZ31 Magnesium Wires, *Key Eng. Mater.* 926 (2022) 389–400, <https://doi.org/10.4028/p-lm7s8y>.
- [35] N. Dodyim, K. Yoshida, T. Murata, Y. Kobayashi, Drawing of magnesium fine wire and medical application of drawn wire, *Procedia Manuf* 50 (2020) 271–275, <https://doi.org/10.1016/j.promfg.2020.08.050>.
- [36] H. Yetiş, D. Avci, F. Karaboğa, D. Gajda, M. Akdoğan, İ. Belenli, An innovative approach to fabricate MgB2/Fe IMD wires by magnesium powder method, *Physica B* 593 (2020), <https://doi.org/10.1016/j.physb.2020.412277>.
- [37] L.X. Sun, J. Bai, F. Xue, L. Tao, C.L. Chu, J. Meng, Exceptional texture evolution induced by multi-pass cold drawing of magnesium alloy, *Mater. Des.* 135 (2017) 267–274, <https://doi.org/10.1016/j.matdes.2017.09.027>.
- [38] M. Shahzad, L. Wagner, Influence of extrusion parameters on microstructure and texture developments, and their effects on mechanical properties of the magnesium alloy AZ80, *Mater. Sci. Eng., A* 506 (2009) 141–147, <https://doi.org/10.1016/j.msea.2008.11.038>.
- [39] M. Shahzad, A.H. Qureshi, H. Waqas, N. Hussain, Influence of Degree of Deformation on Anisotropy in Mechanical Properties in Wrought Magnesium Alloy ZK60, *Key Eng. Mater.* 510–511 (2012) 554–559, <https://doi.org/10.4028/www.scientific.net/KEM.510-511.554>.
- [40] H.L. Ding, X.B. Shi, Y.Q. Wang, G.P. Cheng, S. Kamado, Texture weakening and ductility variation of Mg-2Zn alloy with CA or RE addition, *Mater. Sci. Eng., A* 645 (2015) 196–204, <https://doi.org/10.1016/j.msea.2015.08.025>.
- [41] Y.F. Chai, B. Jiang, J.F. Song, Q.H. Wang, H. Gao, B. Liu, G.S. Huang, D.F. Zhang, F. S. Pan, Improvement of mechanical properties and reduction of yield asymmetry of extruded Mg-Sn-Zn alloy through Ca addition, *J. Alloy. Compd.* 782 (2019) 1076–1086, <https://doi.org/10.1016/j.jallcom.2018.12.109>.
- [42] C. Ha, J. Bohlen, X. Zhou, H.G. Brokmeier, K.U. Kainer, N. Schell, D. Letzig, S. Yi, Texture development and dislocation activities in Mg-Nd and Mg-Ca alloy sheets, *Mater. Charact.* 175 (2021), <https://doi.org/10.1016/j.jmatchar.2021.111044>.
- [43] J.P. Hadorn, K. Hantzsch, S. Yi, J. Bohlen, D. Letzig, J.A. Wollmershauser, S.R. Agnew, Role of Solute in the Texture Modification During Hot Deformation of Mg-Rare Earth Alloys, *Metall. Mater. Trans. A* 43 (2011) 1347–1362, <https://doi.org/10.1007/s11661-011-0923-5>.
- [44] Asgari, M.; Hang, R.; Wang, C.; Yu, Z.; Li, Z.; Xiao, Y. Biodegradable Metallic Wires in Dental and Orthopedic Applications: A Review. *Metals* **2018**, 8, 10.3390/met8040212.
- [45] A. Mosayyebi, D. Lange, Q. Yann Yue, B.K. Somani, X. Zhang, C. Manes, D. Carugo, Reducing deposition of encrustation in ureteric stents by changing the stent architecture: A microfluidic-based investigation, *Biomicrofluidics* 13 (2019), <https://doi.org/10.1063/1.5059370>.
- [46] E. Meza-Garcia, J. Bohlen, S. Yi, D. Letzig, V. Krausel, D. Landgrebe, K.U. Kainer, Influence of alloying elements and extrusion process parameter on the recrystallization process of Mg-Zn alloys, *Mater. Today-Proc.* 2 (2015) 19–25, <https://doi.org/10.1016/j.matpr.2015.05.004>.
- [47] Bohlen, J.; Meyer, S.; Wiese, B.; Lutheringer-Feyerabend, B.J.C.; Willumeit-Römer, R.; Letzig, D. Alloying and Processing Effects on the Microstructure, Mechanical Properties, and Degradation Behavior of Extruded Magnesium Alloys Containing Calcium, Cerium, or Silver. *Materials* **2020**, 13, 10.3390/ma13020391.
- [48] J. Isakovic, J. Bohlen, N. Ben Khalifa, K.U. Kainer, Microstructure Development of Magnesium Alloys AZ31 and AZ80 Due to Temperature Evolution During Direct Extrusion, *Extrusion Technology*, Orlando, Florida, USA, 2022.
- [49] S.B. Yi, H.G. Brokmeier, D. Letzig, Microstructural evolution during the annealing of an extruded AZ31 magnesium alloy, *J. Alloy. Compd.* 506 (2010) 364–371, <https://doi.org/10.1016/j.jallcom.2010.07.008>.
- [50] Dobron, P.; Drozdenco, D.; Horvath Fekete, K.; Olejnak, J.; Bohlen, J. Grain Size-Related Strengthening and Softening of a Precompressed and Heat-Treated Mg-Zn-Ca Alloy. *Materials* **2020**, 13, 10.3390/ma13020351.
- [51] P. Dobron, F. Chmelik, S.B. Yi, K. Parfenenko, D. Letzig, J. Bohlen, Grain size effects on deformation twinning in an extruded magnesium alloy tested in compression, *Scr. Mater.* 65 (2011) 424–427, <https://doi.org/10.1016/j.scriptamat.2011.05.027>.
- [52] B. Wiese, R. Willumeit-Römer, D. Letzig, J. Bohlen, Alloying effect of silver in magnesium on the development of microstructure and mechanical properties by indirect extrusion, *J. Magnesium Alloys* 9 (2021) 112–122, <https://doi.org/10.1016/j.jma.2020.08.001>.
- [53] M.R. Barnett, Twinning and the ductility of magnesium alloys Part I: “Tension” twins, *Mater. Sci. Eng., A* 464 (2007) 1–7, <https://doi.org/10.1016/j.msea.2006.12.037>.
- [54] S.K. Woo, R. Pei, T. Al-Samman, D. Letzig, S. Yi, Plastic instability and texture modification in extruded Mg-Mn-Nd alloy, *J. Magnesium Alloys* 10 (2022) 146–159, <https://doi.org/10.1016/j.jma.2021.07.003>.
- [55] H.-Y. Song, Y.-L. Li, Effect of twin boundary spacing on deformation behavior of nanotwinned magnesium, *Phys. Lett. A* 376 (2012) 529–533, <https://doi.org/10.1016/j.physleta.2011.11.025>.
- [56] H. Somekawa, A. Singh, C.A. Schuh, Effect of twin boundaries on indentation behavior of magnesium alloys, *J. Alloy. Compd.* 685 (2016) 1016–1023, <https://doi.org/10.1016/j.jallcom.2016.06.267>.
- [57] B.L. Mordike, T. Ebert, Magnesium - Properties - applications - potential, *Mater. Sci. Eng., A* 302 (2001) 37–45, [https://doi.org/10.1016/S0921-5093\(00\)01351-4](https://doi.org/10.1016/S0921-5093(00)01351-4).
- [58] Zhang, L.; Wu, X.; Zhang, X.; Yang, X.; Li, Y. Constitutive Model and Recrystallization Mechanism of Mg-8.7Gd-4.18Y-0.42Zr Magnesium Alloy during Hot Deformation. *Materials* (2022), 15, 10.3390/ma15113914.

- [59] D.H. Lee, Y.J. Kim, S.H. Kim, B.G. Moon, S.H. Park, Extrusion limit diagram of AZ91–0.9Ca–0.6Y–0.5MM alloy and effects of extrusion parameters on its microstructure and mechanical properties, *J. Magnesium Alloys* (2021), <https://doi.org/10.1016/j.jma.2021.06.002>.
- [60] B. Wu, J. Li, L. Liu, X. Chen, J. Tan, J. Song, M. Rashad, F. Pan, Effect of Zener-Hollomon Parameter on High-Temperature Deformation Behaviors of Mg–6Zn–1.5Y–0.5Ce–0.4Zr Alloy, *Acta Metallurgica Sinica (English Letters)* 34 (2020) 606–616, <https://doi.org/10.1007/s40195-020-01163-4>.
- [61] F. Cao, C. Sun, S. Liu, J. Liang, R. Liu, H. Guo, N. Guo, Microstructures, hot tensile deformation behavior and constitutive modeling in a superlight Mg–2.76Li–3Al–2.6Zn–0.39Y alloy, *J. Alloy. Compd.* 896 (2022), <https://doi.org/10.1016/j.jallcom.2021.163049>.
- [62] Y. Uematsu, K. Tokaji, M. Kamakura, K. Uchida, H. Shibata, N. Bekku, Effect of extrusion conditions on grain refinement and fatigue behaviour in magnesium alloys, *Mater. Sci. Eng., A* 434 (2006) 131–140, <https://doi.org/10.1016/j.msea.2006.06.117>.
- [63] J. Harmuth, B. Wiese, J. Bohlen, T. Ebel, R. Willumeit-Römer, Wide Range Mechanical Customization of Mg–Gd Alloys With Low Degradation Rates by Extrusion, *Front. Mater.* 6 (2019), <https://doi.org/10.3389/fmats.2019.00201>.
- [64] B.P. Zhang, L. Geng, L.J. Huang, X.X. Zhang, C.C. Dong, Enhanced mechanical properties in fine-grained Mg–1.0Zn–0.5Ca alloys prepared by extrusion at different temperatures, *Scr. Mater.* 63 (2010) 1024–1027, <https://doi.org/10.1016/j.scriptamat.2010.07.038>.
- [65] I.L. Dillamore, W.T. Roberts, Preferred Orientation in Wrought and Annealed Metals, *Metallurgical Reviews* 10 (2013) 271–380, <https://doi.org/10.1179/mtrl.1965.10.1.271>.
- [66] N. Stanford, M.R. Barnett, The origin of “rare earth” texture development in extruded Mg-based alloys and its effect on tensile ductility, *Mater. Sci. Eng., A* 496 (2008) 399–408, <https://doi.org/10.1016/j.msea.2008.05.045>.
- [67] X.S. Huang, K. Suzuki, Y. Chino, M. Mabuchi, Influence of rolling temperature on static recrystallization behavior of AZ31 magnesium alloy, *J. Mater. Sci.* 47 (2012) 4561–4567, <https://doi.org/10.1007/s10853-012-6314-5>.
- [68] K. Hantzsche, J. Bohlen, J. Wendt, K.U. Kainer, S.B. Yi, D. Letzig, Effect of rare earth additions on microstructure and texture development of magnesium alloy sheets, *Scr. Mater.* 63 (2010) 725–730, <https://doi.org/10.1016/j.scriptamat.2009.12.033>.
- [69] I. Basu, T. Al-Samman, Hierarchical Twinning Induced Texture Weakening in Lean Magnesium Alloys, *Front. Mater.* 6 (2019), <https://doi.org/10.3389/fmats.2019.00187>.
- [70] X. Zeng, P. Minarik, P. Dobron, D. Letzig, K.U. Kainer, S. Yi, Role of deformation mechanisms and grain growth in microstructure evolution during recrystallization of Mg–Nd based alloys, *Scr. Mater.* 166 (2019) 53–57, <https://doi.org/10.1016/j.scriptamat.2019.02.045>.
- [71] N. Stanford, The effect of rare earth elements on the behaviour of magnesium-based alloys: Part 2 – recrystallisation and texture development, *Mater. Sci. Eng., A* 565 (2013) 469–475, <https://doi.org/10.1016/j.msea.2012.10.084>.
- [72] D. Panda, R.K. Sabat, S. Suwas, V.D. Hiwarkar, S.K. Sahoo, Texture weakening in pure magnesium during grain growth, *Phil. Mag.* 99 (2019) 1362–1385, <https://doi.org/10.1080/14786435.2019.1581382>.
- [73] S.R. Agnew, M.H. Yoo, C.N. Tome, Application of texture simulation to understanding mechanical behavior of Mg and solid solution alloys containing Li or Y, *Acta Mater.* 49 (2001) 4277–4289, [https://doi.org/10.1016/S1359-6454\(01\)00297-X](https://doi.org/10.1016/S1359-6454(01)00297-X).
- [74] V.M. Miller, T.D. Berman, I.J. Beyerlein, J.W. Jones, T.M. Pollock, Prediction of the plastic anisotropy of magnesium alloys with synthetic textures and implications for the effect of texture on formability, *Mater. Sci. Eng., A* 675 (2016) 345–360, <https://doi.org/10.1016/j.msea.2016.08.063>.
- [75] J. Bohlen, M.R. Nurnberg, J.W. Senn, D. Letzig, S.R. Agnew, The texture and anisotropy of magnesium–zinc–rare earth alloy sheets, *Acta Mater.* 55 (2007) 2101–2112, <https://doi.org/10.1016/j.actamat.2006.11.013>.
- [76] J. Victoria-Hernandez, S.B. Yi, D. Klamunzer, D. Letzig, Comparison of the Mechanical Properties and Forming Behavior of Two Texture-Weakened Mg–Sheet Alloys Produced by Twin Roll Casting, *Front. Mater.* 6 (2019), <https://doi.org/10.3389/fmats.2019.00288>.
- [77] E.O. Hall, The Deformation and Ageing of Mild Steel: III Discussion of Results. *Proceedings of the Physical Society. Section B* 1951, 64, 747–753, 10.1088/0370-1301/64/9/303.
- [78] N.J. Petch, The Cleavage Strength of Polycrystals, *J. Iron Steel Inst.* 174 (1953) 25–28.
- [79] X. Liu, J.J. Jonas, L.X. Li, B.W. Zhu, Flow softening, twinning and dynamic recrystallization in AZ31 magnesium, *Mater. Sci. Eng., A* 583 (2013) 242–253, <https://doi.org/10.1016/j.msea.2013.06.074>.
- [80] A. Baczmanski, M. Wronski, P. Kot, S. Wronski, A. Labaza, K. Wierzbanski, A. Ludwik, M. Marciszko-Wiackowska, The role of basal slip in the generation of intergranular stresses in magnesium alloy studied using X-ray diffraction and modelling, *Mater. Des.* 202 (2021), <https://doi.org/10.1016/j.matdes.2021.109543> 109543.
- [81] S.R. Agnew, O. Duygulu, Plastic anisotropy and the role of non-basal slip in magnesium alloy AZ31B, *Int. J. Plast.* 21 (2005) 1161–1193, <https://doi.org/10.1016/j.ijplas.2004.05.018>.
- [82] D.B. Xia, X. Chen, G.S. Huang, B. Jiang, A.T. Tang, H. Yang, S. Gavras, Y.D. Huang, N. Hort, F.S. Pan, Calculation of Schmid factor in Mg alloys: Influence of stress state, *Scr. Mater.* 171 (2019) 31–35, <https://doi.org/10.1016/j.scriptamat.2019.06.014>.